Interaction between colloidal particles on an oil–water interface in dilute and dense phases

2015 J. Phys.: Condens. Matter 27 194119

(http://iopscience.iop.org/0953-8984/27/19/194119)

IOP Publishing Journal of Physics: Condensed Matter
J. Phys.: Condens. Matter **27** (2015) 194119 (11pp) doi:10.1088/0953-8984/27/19/194119

Interaction between colloidal particles on an oil–water interface in dilute and dense phases

Lucia Parolini[1], Adam D Law[2,3], Armando Maestro[1], D Martin A Buzza[4] and Pietro Cicuta[1]

[1] Cavendish Laboratory, University of Cambridge, The Old Schools, Trinity Ln, Cambridge CB2 1TN, UK
[2] Max-Planck-Institut für Intelligente Systeme, Heisenbergstr. 3, D-70569 Stuttgart, Germany
[3] IV. Institut für Theoretische Physik, Universität Stuttgart, Pfaffenwaldring 57, D-70569 Stuttgart, Germany
[4] Department of Physics and Mathematics, Theory of Condensed Matter Group, The University of Hull, Hull, HU6 7RX, UK

E-mail: D.M.Buzza@hull.ac.uk and pc245@cam.ac.uk

Received 20 September 2014, revised 6 November 2014
Accepted for publication 18 November 2014
Published 29 April 2015

Abstract

The interaction between micron-sized charged colloidal particles at polar/non-polar liquid interfaces remains surprisingly poorly understood for a relatively simple physical chemistry system. By measuring the pair correlation function $g(r)$ for different densities of polystyrene particles at the decane–water interface, and using a powerful predictor–corrector inversion scheme, effective pair-interaction potentials can be obtained up to fairly high densities, and these reproduce the experimental $g(r)$ in forward simulations, so are self consistent. While at low densities these potentials agree with published dipole–dipole repulsion, measured by various methods, an apparent density dependence and long range attraction are obtained when the density is higher. This condition is thus explored in an alternative fashion, measuring the local mobility of colloids when confined by their neighbors. This method of extracting interaction potentials gives results that are consistent with dipolar repulsion throughout the concentration range, with the same magnitude as in the dilute limit. We are unable to rule out the density dependence based on the experimental accuracy of our data, but we show that incomplete equilibration of the experimental system, which would be possible despite long waiting times due to the very strong repulsions, is a possible cause of artefacts in the inverted potentials. We conclude that to within the precision of these measurements, the dilute pair potential remains valid at high density in this system.

Keywords: colloids at interfaces, two dimensional, liquid interfaces, electrostatic interactions

(Some figures may appear in colour only in the online journal)

1. Introduction

Charged colloidal particles confined to an oil–water interface have attracted significant attention since Pieranski showed that they exhibit strong two-dimensional confinement and long range electrostatic repulsion [1]. Particles are so effective at stabilizing fluid interfaces [2] that they prevent [3] or tune [4] coalescence in emulsions. Polystyrene and silica micron-sized spheres have been often studied, and are the typical model systems. They can be deposited on the interface between water and an alkane, where they exhibit a repulsive interaction that is orders of magnitude stronger than, and qualitatively different

from, the interparticle potential that those same particles have in the bulk aqueous phase. In the bulk, the interaction is always sub-micron ranged, and fairly well described by the DLVO form [5]. In stark contrast, the repulsion energy between particles on water/oil interfaces can be greater than thermal energy at distances of tens of micrometers.

The puzzle of particle interaction on surfaces has been the object of extensive experimental and theoretical work: optical tweezers measurements of the pair interaction potential have shown clear dipolar repulsion [6] in dilute conditions, and have highlighted many-body effects, appearing at very close range in the formation of small particle clusters, attributed to capillarity [7, 8]. On the theoretical side, interparticle interaction has been estimated with increasingly sophisticated arguments: the linearized Poisson–Boltzmann theory, for two charged particles near an interface between phases with different dielectric constants, was solved in [9, 10]; non-linear effects were addressed by Oettel and Dietrich [11]. Other subtle effects such as possible charges on the oil side [12] and finite ion size have also been considered [7]. All these potentials are repulsive, of approximately dipole–dipole form, and efforts have been directed at understanding the amplitude of this interaction.

A few experiments in the literature have hinted at more complex shapes of the potential, including stable long range clusters [13], and long range (but shallow) minima [14]. Various experiments are discussed in [15] where several sources of interaction are also overviewed. *Short ranged* minima in the pair potential of interfacial particles have also been reported, and are easier to account for: in optical trap experiments [16] an attraction range of around 4 or 5 μm was seen, and attributed to capillarity, while the presence of a deep ($\gg k_B T$) minimum was reported in [17] based on AFM measurements, and attributed to anisotropy in the charge distribution on the colloid surface giving rise to in-plane dipoles (this interpretation was then criticized in [18]). In these last two reports the range of attraction is just a few microns which, while still remarkable with respect to dispersion forces and generally DLVO theory, is much smaller than the tens of micrometers reported in [13, 14]. Large particles (over $\sim$50 μm for typical materials) can individually indent the surface [19], or impose undulations [20, 21], giving rise to long-range interaction, but these processes are not expected for micron-sized colloids. Small colloids might still interact long range, via undulations coming from a pinned rough contact line [15]. One should also consider that most experimental techniques one can use on colloidal scale particles are only able (either intrinsically or through averaging of pairs at random orientation) to measure the radially averaged pair interaction, and this can hide the details of an underlying anisotropic interaction.

Our aim in this work is to explore the interaction potential of small particles, beyond the dilute regime, and verify if the pair potential measured in the dilute phase still holds with increasing density. While the experiments appear at first as relatively straightforward, obtaining reliable potentials in the concentrated regime is difficult, and indeed we present two methods of doing this. We discuss why measuring the potential from particle fluctuations around their mean position is a better way of approaching the experimental data in the dense regime, and we show that the results of this method agree with the dilute limit pair potential.

2. Materials and methods

2.1. Chemicals

The oil–water interface has to be very clean; following previous protocols, we worked with n-decane (Across Organics, 99+%) and ultrapure water (Elga) of resistivity >18 MΩcm. Following standard protocol, the decane was cleaned by twice passing through an aluminium oxide powder column, as in [22–24], to remove polar components, followed by distillation.

The particles studied are surfactant-free, negatively charged (sulphate surface groups) polystyrene (PS) spherical particles (radius $r = 1$ μm) from Invitrogen Molecular Probes, supplied as aqueous suspension (solid%: 3.1). These particles are re-suspended in ultrapure Elga water, then on the day of experiments they are diluted between 50 and 500 times in water, and further mixed with isopropanol to a ratio 3:2 water:isopropanol. Isopropanol, used as-received, serves to promote the spreading of particles at the interface, as in [25], and dissolves in the aqueous phase without practically changing the interfacial tension (the volume of the isopropanol added is about 0.1% of the total volume of the aqueous phase).

2.2. Assembling the particle monolayer

PS particle monolayers at the decane-water interface were prepared in a glass-bottom imaging petri dish (50 mm diameter, MatTek Corporation), for observation with an inverted microscope. The aqueous subphase was poured first (to a thickness $\sim$5 mm), then the decane layer (2 or 3 mm thickness) was carefully deposited onto the water phase. The particles in the isopropanol-water spreading solution were added to the interface by dropping small drops ($\approx$1 μl) from a Hamilton micro-syringe, into the oil phase about 1 mm above the interface. Finally the petri-dish was covered[5].

The three-phase fluid/particle contact angle depends on the spreading and interface conditions [26] and is very difficult to probe directly *in situ*, and different techniques have been used to estimate this parameter [27]. In conditions close to this work, optical observations [12] or interferometry [28] were possible on larger spheres, whereas on micrometer scale spheres at decane-water (or aqueous phase) interface there is data from a gel trapping technique [29] that measured 111°±4° and 101° ± 3°, freeze-fracture measuring 85° ± 5.2°, and gel trapping combined with AFM that gives 122° ± 4° [30]. All

[5] Despite the enclosure, the absence of vibrations and the long equilibration times (room T equilibration times of up to 12 h, and at least 1 h, were allowed before recording) there is invariably drift on the surface. This is well known in this type of experiment, and very difficult to remove due to the volatility of the oil phase; it brings some limitations, e.g. on the longest time each particle can be observed, but overall it is useful in that independent configurations of the system can be observed without moving the stage (which would itself perturb the interface).

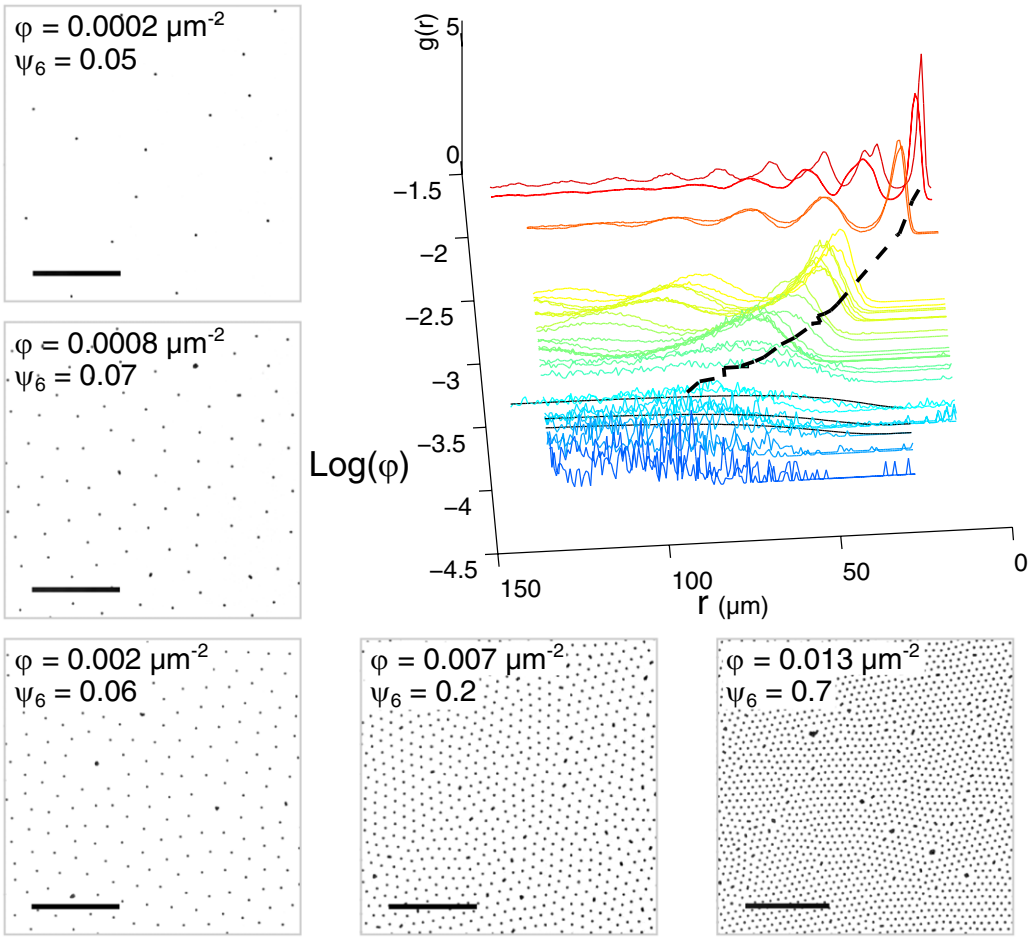

Figure 1. The particle monolayer is studied by optical microscopy over a range of coverage, illustrated by the representative images (scale bars 100 μm). The pair correlation functions $g(r)$ show clearly the transition from a dilute regime to a more structured phase in which a peak develops in $g(r)$, with $g(r) > 1$ for some r. Notice how the positions of the first peaks, traced by the dashed line, gradually shift towards smaller values, indicating that the average interparticle distance decreases with increasing surface density.

these values point to the PS latex spheres sitting approximately half way at the decane water interface.

Other work [6, 8] has shown that the stability and structure of these interfacial systems is almost independent on the ionic strength in the subphase.

2.3. Imaging

A Nikon Eclipse microscope, with a 10× dry objective (Plan Apo, NA = 0.45) was used in brightfield transmission mode. Images were recorded on either of two AVT cameras: Pike F-100B (CCD) or Marlin 131B (CMOS). Pixel image size was, respectively, 0.714 and 0.667 μm. Frame rate varied depending on the region of interest captured, in the range between 11 and 60 fps. In this configuration, focusing appropriately, colloidal particles appear as dark dots in a brighter background; contrast is stretched to highlight the particles in figure 1. Using image analysis software developed in house for correlation filtering, sub-pixel resolution of particle positions [31], the position of each particle is obtained, from which the pair correlation function $g(r)$ is calculated for each frame. Particle trajectories are then obtained following standard methods [32]. Around 4000 frames are recorded on each experiment.

2.4. Inversion of pair correlation functions

One method for extracting pair potentials $U(r)$ in colloidal monolayers is to invert their structural data, such as the pair correlation function $g(r)$ and the structure factor $S(\mathbf{q})$. Such inversions are based on integral equation theory and are therefore only valid if the colloidal monolayer is in the fluid phase. Note that the interaction potentials obtained via this route are *effective* pair potentials which may involve three-body and higher-body contributions, especially at higher colloidal densities [33–35]. Specifically, we use a hard-disk predictor-corrector (HDPC) method to carry out the inversion [36], where the bridge correlation function is approximated by a hard disk reference system and solved iteratively. Such a method has been shown to be much more accurate compared to standard hypernetted chain closure (HNC) or Percus–Yevick closure (PY) based inversion schemes whilst being computationally inexpensive and robust with respect to experimentally realistic levels of noise in the input $g(r)$ data [36, 37]. We use *both* the $g(r)$ and $S(\mathbf{q})$ as the input data for the HDPC method in order to avoid numerical errors that are often encountered when performing numerical Fourier transforms [38, 39]. The input $g(r)$ and $S(\mathbf{q})$ curves are calculated directly from particle coordinates obtained from experimental micrographs and are

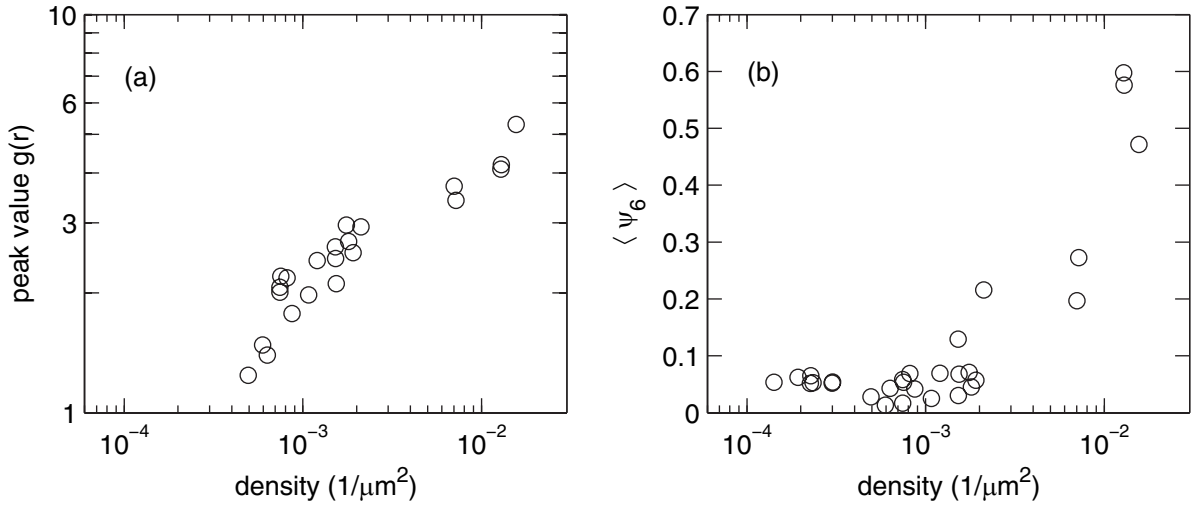

Figure 2. The colloid particle layer is studied in dilute and solid phases, as characterised by two measures. (*a*) The height of the $g(r)$ peak at $r = a$; (*b*) the mean value of angular order ψ_6, averaged over all particles.

averaged over multiple snapshots. In order to check that the inverted potentials are self-consistent with the input $g(r)$, we perform forward Monte Carlo simulations of the inverted potentials to see if they reproduce the input $g(r)$.

3. Results

3.1. Structure and inversions

Colloidal particles at interfaces are strongly confined to the plane, and can arrange into states of differing order, depending on the density of particles, measured in terms of the number density $\varphi = N/A$. At very low density, particles are in a disordered 'gas' phase; this can be seen in the pair correlation $g(r)$ data, which tend to unity smoothly from below in figure 1. Increasing density, at around the density $\varphi \simeq 5 \times 10^{-4}\,\mu\text{m}^{-2}$ (i.e. $a = 48\,\mu\text{m}$ assuming already a hexagonal lattice of spacing a), a peak develops in the $g(r)$, indicating the onset of some translational order, as shown in figure 2(*a*). From the density of $4 \times 10^{-4}\,\mu\text{m}^{-2}$, the average inter-particle distance (measured as the position of the $g(r)$ peak) scales inversely with the square root of density, and the proportionality factor is $(2/\sqrt{(3)})^{0.5}$ as expected for a hexagonal structure. From around the same density, the angular order parameter ψ_6 also becomes finite, as shown in figure 2(*b*), identifying the crystallisation concentration to be $\varphi_c \approx 2 \times 10^{-3}\,\mu\text{m}^{-2}$ (i.e. $a \approx 24\,\mu\text{m}$).

For densities below the the crystallization density φ_c, the monolayer exists in the fluid phase and we can therefore obtain the pair potential between colloids $U(r)$ by inverting the pair correlation function $g(r)$. In the ultra-dilute regime, the pair potential can be approximated by the potential of mean force and can therefore be calculated from

$$g\,(r) = \mathrm{e}^{-U(r)/k_\mathrm{B}T}. \tag{1}$$

For low density colloidal samples ($\varphi = 2\times10^{-4}\,\mu\text{m}^{-2}$), fitting the pair interaction potential obtained from equation (1) to the form $U\,(r) = k_\mathrm{B}T\,A\,r^{-\alpha}$ gives $\alpha = 2.94$, confirming the dipolar pair interaction potential between the particles for low density. Fixing $\alpha = 3$ gives $A \simeq 1.8 \pm 0.8 \times 10^5\,\mu\text{m}^3$. This value is in broad agreement with published results of other groups, for example in [7] the dipolar repulsion was measured both with optical tweezers ($A = 1.3\pm0.5\times10^5\,\mu\text{m}^3$) and through the pair correlation function ($A = 0.5 \pm 0.5 \times 10^5\,\mu\text{m}^3$). The same group reported stronger repulsion in [8] ($A = 5.1 \pm 2.4 \times 10^5\,\mu\text{m}^3$) and attributed that to stronger charges on the particles; interactions measured on individual pairs showed a fairly broad scatter, of one order of magnitude. Earlier work with optical tweezers on slightly larger particles had measured $A \simeq 4 \times 10^5\,\mu\text{m}^3$ [6].

Equation (1) is only valid in the ultra-dilute regime. In order to obtain the interaction potential across the entire range of colloidal densities, we use the HDPC inversion scheme [36] introduced in section 2.4. Figure 3(*b*) shows in panels (ii) and (iii) the interaction potentials $U\,(r)\,/k_\mathrm{B}T$ obtained using this method for two densities $\varphi < \varphi_c$. The inverted pair potentials clearly show density-dependent behavior: while at low densities (i), the pair interaction potential is a dipole–dipole repulsion (analysis of equation (1)), at higher densities a minimum develops (as also detected via similar methods in [40]), becoming deeper and shifting to smaller distances as the density increases.

We will discuss this apparent density dependence in just a moment. However, we first seek to parameterise these inverted pair potential using a convenient phenomenological form; this will be very helpful for our subsequent theoretical analyses. For the lowest density samples where the pair potential is dipolar, we use the simple parametrisation

$$\frac{U(r)}{k_\mathrm{B}T} = \frac{A}{r^3} \tag{2}$$

while for the higher density samples where the pair potential develops a minimum, we use the more complicated phenomenological parametrisation

$$\frac{U(r)}{k_\mathrm{B}T} = \frac{A}{r^3} - \frac{B}{r^2} + \frac{1}{r^2}\frac{\alpha}{\exp\left[\gamma(r_0 - r)\right] + 1}. \tag{3}$$

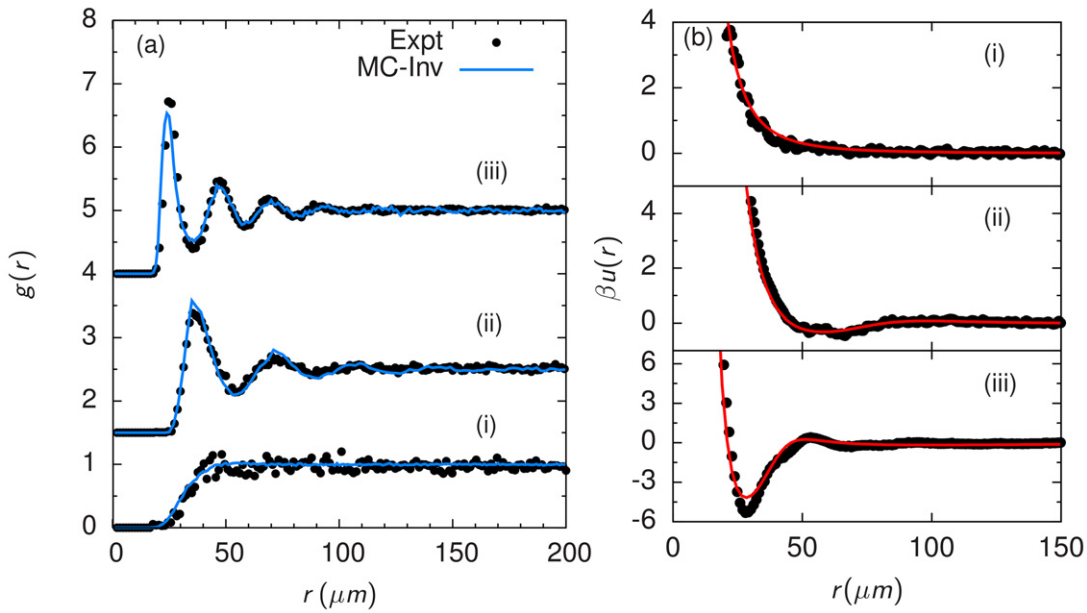

Figure 3. (*a*) Comparison between radial distribution functions $g(r)$ obtained from experimental micrographs of the colloidal monolayers (•) and Monte Carlo (MC) simulations of the corresponding parameterised inverted potentials shown in (*b*) (lines) for three different number densities: (i) $\varphi = 2.2 \times 10^{-4}\ \mu\text{m}^{-2}$, (ii) $\varphi = 7.3 \times 10^{-4}\ \mu\text{m}^{-2}$ and, (iii) $\varphi = 1.8 \times 10^{-3}\ \mu\text{m}^{-2}$. (*b*) In (i) potential obtained from the potential of mean force (•), fitted with a dipolar repulsion. In (ii) and (iii), comparison between the pair potentials obtained from the HDPC inversion of the experimental $g(r)$ data shown in (*a*) (•), and the corresponding parametrisation of these inverted potentials using equation (3) and table 1 (solid lines).

Table 1. Fitting parameters in equation (3) used to parameterise the inverted potentials of the colloidal monolayer at different densities.

Density/μm^{-2}	$A/\mu\text{m}^3$	$B/\mu\text{m}^2$	$\alpha/\mu\text{m}^2$	$\gamma/\mu\text{m}^{-1}$	$r_0/\mu\text{m}$
7.3×10^{-4}	$3.1 \pm 0.7 \times 10^5$	$7 \pm 2 \times 10^3$	$5 \pm 2 \times 10^3$	0.11 ± 0.03	77 ± 1
1.05×10^{-3}	$2.2 \pm 0.1 \times 10^5$	$6.7 \pm 0.4 \times 10^3$	$5.2 \pm 0.4 \times 10^3$	0.11 ± 0.04	60 ± 4
1.8×10^{-3}	$3.27 \pm 0.04 \times 10^5$	$1.58 \pm 0.03 \times 10^4$	$1.08 \pm 0.03 \times 10^4$	0.22 ± 0.02	39.4 ± 0.2
2.2×10^{-3}	$2.40 \pm 0.01 \times 10^5$	$1.20 \pm 0.05 \times 10^4$	$8.4 \pm 0.8 \times 10^4$	0.29 ± 0.05	34.8 ± 0.8

where A, B, α, γ and r_0 are fitting parameters. The first term in equation (3) generates dipolar behaviour at small r, the second term produces a minimum in the potential and the third term, which contains a Fermi–Dirac-like cut-off function, ensures that the pair potential decays rapidly to zero at long distances. The combination in equation (3) is to be thought of as an empirical fit to the data, and our main purpose is to have a convenient smooth function that works well enough fitting the data that we can then use it in 'forward' simulations; the terms, particularly the second and third term, are not intended to model an underlying physical process.

In figure 3(*b*), we plot the parameterised potentials for different densities (curves) and we see that they accurately represent all the key features of the original inverted potentials (•). The fitting procedure used to obtain these parameters for the higher density samples was as follows. The small r data was first fitted to the first two terms to obtain A and B. The residuals were then fitted to the third term to obtain the remaining parameters α, γ and r_0. The fitting parameters for the different densities studied are given in table 1. We note that the values of A obtained from these higher density samples are consistent with the value A determined from dilute sample analysis and with previous measurements of the dipole strength for this system.

In order to check the reliability of the inversion scheme, we performed forward Monte Carlo simulations based on these parameterised potentials. In figure 3(*a*), we compare the $g(r)$ calculated from these simulations (curves) with the original input $g(r)$ (•) for different densities and see that there is excellent agreement between the two, thus confirming that the inverted potentials are self-consistent with the input $g(r)$ up to the crystallization density.

We now turn our attention to the origin of the apparent density dependent attractive well in our colloidal systems at higher densities. One possible explanation for this behaviour is that it could be a signature of many body effects. As discussed earlier, the interaction potentials obtained via the inversion of $g(r)$ are *effective* pair potentials which may involve three-body and higher-body contributions at higher colloidal densities that lead to a density dependent attraction in the pair potentials [33–35]. However, such an effect could also arise as an artefact of the system becoming increasingly non-ergodic on experimental timescales, as we approach the crystallization point; the input $g(r)$ might no longer reflect *equilibrium* structure (see section 3.3). For such non-ergodic systems, the pair potentials obtained via the inversion of $g(r)$ no longer accurately represent the underlying pair potentials.

A more accurate method for determining the pair potential in the non-ergodic regime is to measure the mean squared displacement (msd) of particles as a function of the average spacing between particles. This is the subject of the next section. As we shall see later, harmonic lattice theory calculations of the msd based on a dipolar potential with the same magnitude as in the dilute limit appear to yield better agreement with the experimental data compared to the density dependent pair potentials, suggesting that the underlying interaction potential at high densities may in fact be dipolar and density independent. However as the msd calculations based on the density dependent pair potentials lie within the error bounds of the dipolar repulsion fluctuations, unfortunately on this very intriguing point, we do not feel that the msd calculations allow us to categorically rule out (or confirm) the presence of long range attraction.

3.2. Fluctuation dynamics

The dynamics of a colloidal particle can be characterized by measuring the mean square displacement (msd) of the particle, defined for each directional component as the time average:

$$\Delta^2(\tau) = \langle (x(t+\tau) - x(t))^2 \rangle_t \tag{4}$$

where $x(t)$ is the x coordinate of the particle at time t. We shall refer to the msd defined in equation (4) as the *dynamic* msd. The dynamic msd characterizes the kind of motion exhibited by the particle, allowing to distinguish between free (Brownian) motion where $\Delta^2(\tau) = 2D_0\tau$ (where D_0 is the diffusion coefficient and τ the lag time), from restricted motion where the square displacement grows sublinearly or even plateaus at large τ for strong confinement. In general the features that characterize the motility regimes depend strongly on the details of the interaction, and on the density of the system. The case of particles confined within a *fixed* harmonic potential is particularly relevant, since it is a good approximation to motions in local minima over short timescales, such as the fluctuations around the equilibrium lattice positions in colloidal crystals. An expression for the dynamic msd for such a system was derived by Pusey and van Megen [41], which is given by

$$\Delta^2(\tau) = 2\langle \Delta x^2 \rangle \left[1 - \exp\left(-\frac{D_0\tau}{\langle \Delta x^2 \rangle} \right) \right] \tag{5}$$

where $\langle \Delta x^2 \rangle$ is the mean squared x-displacement of the particle from its equilibrium lattice position. We shall refer to $\langle \Delta x^2 \rangle$ as the *equilibrium* msd. Equation (5) predicts that the dynamic msd $\Delta^2(\tau)$ plateaus exponentially with time to twice the equilibrium msd.

When considering particle fluctuations in a *two-dimensional* colloidal crystal, an important technical complication is the fact that the msd of a particle from its equilibrium position diverges logarithmically with system size in two dimensions [42]. However Bedanov *et al* [43] and later Zheng and Earnshaw [44] showed that if instead, one defines the msd of a particle with respect to a local reference frame defined by its neighbours, we obtain a well defined quantity for an infinite 2D system. Following Zheng and Earnshaw, we therefore define the equilibrium msd to be the mean squared x-displacement of the colloidal particle from the average x-coordinate of its 6 nearest neighbours, i.e.

$$\langle \Delta x^2 \rangle = \left\langle \left(x_0 - \frac{1}{6}\sum_{l=1}^{6} x_l \right)^2 \right\rangle \tag{6}$$

where x_0 and x_l are the x coordinates of the particle and its l-th nearest neighbour, respectively.

One further complication is that in real colloidal crystals where there are defects, in addition to homogeneous collective drift of particles, there are instances where localized movement occurs along disclination lines [45, 46]. Therefore, when calculating the equilibrium and dynamic msd, in addition to using the local neighbors of each particle as a reference frame, we also remove the small fraction of any outliers with high-mobility.

Representative dynamic msd data as a function of density is shown in figure 4(*a*): At low densities the mean square displacement is linear with time, indicating a diffusive regime; Increasing the density the particles are forced closer, and become caged. The high density data shows a deviation from the diffusive regime (which is still visible, at short lag times, with the same D_0), into a sub-diffusive regime. This deviation happens at ever smaller lag times the greater the surface density. At the highest density presented here, particles are in the sub-diffusive regime already at the smallest lag times. A totally flat plateau, as expected from equation (5), is not observed, most likely because because the cage formed by the particle's six neighbors is itself fluctuating.

We can obtain D_0 and $\langle \Delta x^2 \rangle$ at each monolayer density by fitting the dynamic msd to equation (5). Note that equation (5) is only applicable to particle fluctuations in a colloidal crystal for small lag times τ, when the particle is near the minima of the confining potential which is well approximated by a harmonic potential; at larger lag times, the particle explores regions far from its equilibrium lattice position and begins to 'feel' the anharmonic terms in the confining potential. We therefore fit the dynamic msd at short τ (up to just after the deviation is seen from simple diffusion) to equation (5), to obtain D_0 and $\langle \Delta x^2 \rangle$. Applying this procedure to colloidal monolayers across the entire density range studied, we obtain an average value for the diffusion coefficient $D_0 = 0.28 \pm 0.02\,\mu\mathrm{m}^2\,\mathrm{s}^{-1}$, which is close to $D_0 = 0.23\,\mu\mathrm{m}^2\,\mathrm{s}^{-1}$ expected from the Stokes–Einstein relation (having taken the viscosity as the average of water and decane, the latter 0.000 92 Pa s at 20 °C). By normalising the dynamic msd $\Delta^2(\tau)$ and lag time τ using the fitted values for D_0 and $\langle \Delta x^2 \rangle$, we can define rescaled msd and time variables $\Delta^{*2} = \Delta^2/\langle \Delta x^2 \rangle$ and $\tau^* = D_0\tau/\langle \Delta x^2 \rangle$ and construct a master curve from the dynamic msd curves of the different densities, as shown in figure 4(*b*). The collapse of the data on the master curve is reasonable, with some deviations at the plateau as already discussed earlier. Notwithstanding these deviations, the caging effect is clearly visible at large τ.

The various measurements extracted so far can be brought together in considering the mean displacements of particles in their equilibrium positions, $(\langle \Delta x^2 \rangle)^{0.5}$ versus the lattice

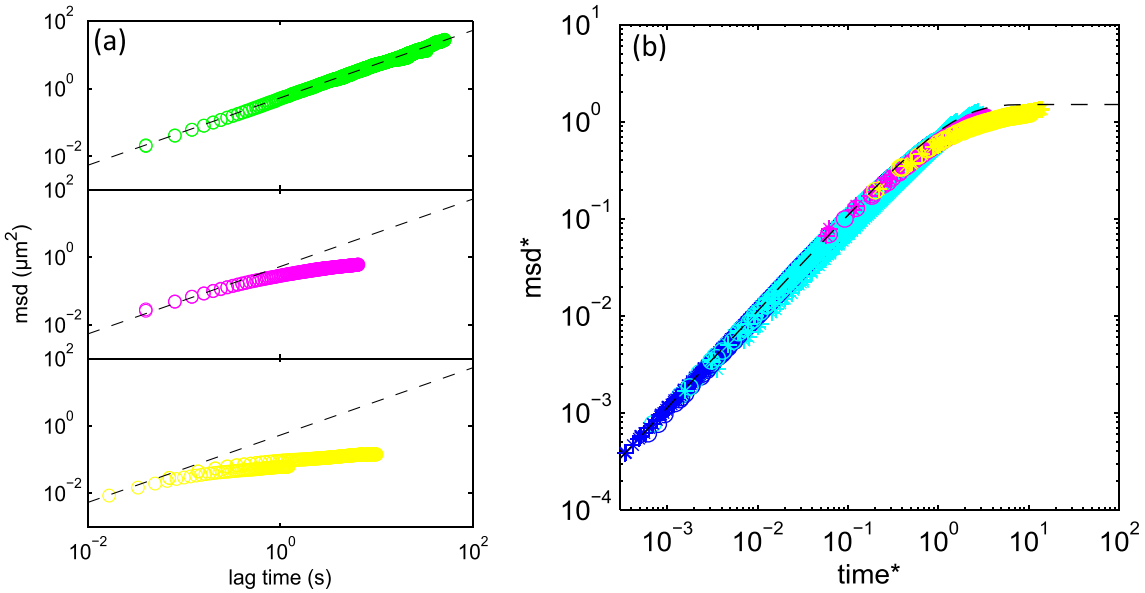

Figure 4. The dynamic mean square displacement (msd) of the particles (evaluated in one dimension) depends on the density and becomes sublinear. (*a*) Example for particles in a dilute ($\varphi < 10^{-4}\ \mu\mathrm{m}^{-2}$), intermediate ($3\times10^{-3} < \varphi < 10^{-2}\ \mu\mathrm{m}^{-2}$) and highly concentrated ($10^{-2} < \varphi < 3\times10^{-2}\ \mu\mathrm{m}^{-2}$) conditions. The dashed lines are a linear dependence of the msd on lag time, fitted on this dilute condition with $D = 0.265\ \mu\mathrm{m}^2\ \mathrm{s}^{-1}$, and shown here to highlight the deviation from linear diffusion at increasing lag time and concentration. (*b*) The master curve is obtained by assuming that the caged particle motion is described by equation (5) up to the lag time where deviations from linear are evident, and rescaling the time and msd variables. The rescaling factors, as described in the text, correspond physically to the diffusion coefficient and the equilibrium msd.

spacing a. This is plotted in figure 5. The equilibrium msd is sensitive to the underlying colloidal interaction, thus providing an independent method for measuring colloidal interactions. We first consider a simple model that assumes that particles only interact with six nearest hexagonal neighbors which are fixed in a plane, and that their interactions are described by a dipole–dipole repulsion $\beta U(r) = A/r^3$. A simple geometrical argument based on balancing the thermal energy with the energy required to displace a particle by Δx relative to the lattice position (i.e. equipartition) yields

$$\langle \Delta x^2 \rangle \simeq \frac{\pi a^5}{72A} = 4.36\times10^{-2}\,\frac{a^5}{A}. \qquad (7)$$

We can rigorously include the interaction of the colloidal particle with all other particles in the colloidal crystals (not just its six nearest neighbours) as well as the fluctuations of these particles into our calculation of the equilibrium msd by using harmonic lattice theory [47, 48], see appendix A. For a dipolar potential, harmonic lattice theory yields

$$\langle \Delta x^2 \rangle = 5.31\times10^{-2}\,\frac{a^5}{A}, \qquad (8)$$

i.e. the equilibrium msd has the same scaling with a and A as in equation (7) but with a modified prefactor (about 20% higher). Using the dipole interaction strength $A \approx 1.8\times10^5\ \mu\mathrm{m}^3$ measured in the dilute regime in equation (8), in figure 5 we compare the predictions of this model with the experimental data for the equilibrium msd. Interestingly, this simple dipole model describes well the msd, especially given that it is a parameter-free fit to the data. In particular, it correctly predicts the slope of $\langle \Delta x^2 \rangle$ versus a curve, suggesting that

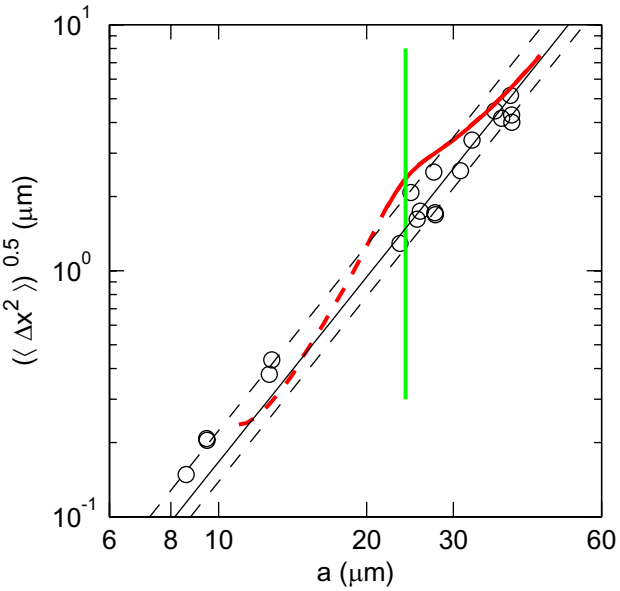

Figure 5. The average displacements from lattice equilibrium positions are related to the interaction potential. The experimental data (○) is consistent both with the potential from the dilute regime (equation (8), solid dark line $A = 1.8\times10^5\ \mu\mathrm{m}^3$, with the lower and upper bounds, i.e. $A = 1.0\times10^5$ and $2.6\times10^5\ \mu\mathrm{m}^3$, dashed), and also with the deviations calculated using harmonic lattice theory using the density dependent potentials with the parameters in table 1; these are plotted as solid line in the region where the inversions are carried out, and as dashed line in the higher density region where we extrapolate the inverted parameters. The repulsive dipole arguably describes the experimental data better, and comes from a simpler physics. The vertical line is at $a = 24\ \mu\mathrm{m}$ which we identify as the crystallisation point from the data of figure 3.

the underlying colloidal interaction may in fact be dipolar and constant in magnitude.

Next we consider the case where the colloids interact with each other via the density dependent pair potentials given by equation (3) and table 1. Specifically, we assume that the dipole term is constant with magnitude given by $A = 2.7 \times 10^5\ \mu\text{m}^3$ (i.e. the average value for A in table 1). For all the other parameters, we assume that their density dependence has a power law form $C\varphi^m$ over the density range studied, with the parameter values C, m determined by fitting to the parameter values given in table 1. The results of this calculation are also shown in figure 5 as the red line. Extrapolating the trends beyond the window of densities in which the inversions were possible, the red line remains within the error bounds of the dipolar repulsion fluctuations. However, the experimental data is arguably closer to the simple dipole calculation as there is no evidence to suggest that the data exhibits the undulations predicted by the density dependent potentials. Comparing both theories, we conclude that the simple repulsive dipole potential as measured in the dilute regime describes the experimental msd data better than the density dependent potentials in figure 3, though we are unable to robustly rule out the density dependent potentials based on the experimental accuracy of the data.

3.3. Issue of structure equilibration

As discussed at the end of section 3.1, one reason for the emergence of the apparent attractive well in the inverted potentials could be as an artefact of the system becoming increasingly non-ergodic on experimental timescales as we approach the crystallization point so that the input $g(r)$ is no longer the *equilibrium* $g(r)$. In order to demonstrate this quantitatively, in appendix B we have estimated the escape time of a particle from the 'cage' formed by its six nearest neighbours as a function of density. We find that the escape time rises very steeply with density. We note in particular that there is a huge increase in τ_{escape} going from $\varphi = 2.25 \times 10^{-4}\ \mu\text{m}^{-2}$ to $\varphi = 7.33 \times 10^{-4}\ \mu\text{m}^{-2}$, the latter being the density where we start to see a minima appearing in the inverted pair potential.

In order to demonstrate that non-ergodicity in the input $g(r)$ can lead to spurious features in the inverted potential, we performed two MC simulations for a colloidal monolayer with system parameters in the range where we observe an attractive well in the inverted potential: particle concentration $\varphi = 1.05 \times 10^{-3}\ \mu\text{m}^{-2}$; particles interact with each other through a purely repulsive dipolar interaction $\beta U(r) = A/r^3$ with $A = 1.8 \times 10^5\ \mu\text{m}^3$. In the first simulation, the maximum trial step length was chosen such that acceptance ratio was equal to the optimum value of 30%. The $g(r)$ and $S(\mathbf{q})$ measurements from the simulations are calculated using 100 snapshots, ensuring that the system is well equilibrated between snapshots. We refer to this simulation as the ergodic simulation. In the second simulation, we keep all other parameters the same as the first simulation, but reduce the maximum trial step length by a factor of 10 and the number of MC steps between snapshots to 1 MC step per particle, so that the simulation no longer explores phase space efficiently. We refer to this simulation as the non-ergodic simulation. From figure 6, we see that the inversion of the $g(r)$ calculated from the ergodic simulation (red points) accurately reproduces the input dipolar interaction. In contrast, the inversion of $g(r)$ calculated from the non-ergodic simulation (blue points) shows an attractive well, with a well depth similar to what is observed in the experimental systems. These simulations demonstrate that non-ergodicity can lead to spurious features in the inverted potential that are not present in the underlying potential. Very long-term imaging experiments (challenging for many reasons, amongst which the need to prevent evaporation of both liquids and avoid sample drift), looking for large scale equilibration times and aging, might be carried out in future to test this scenario.

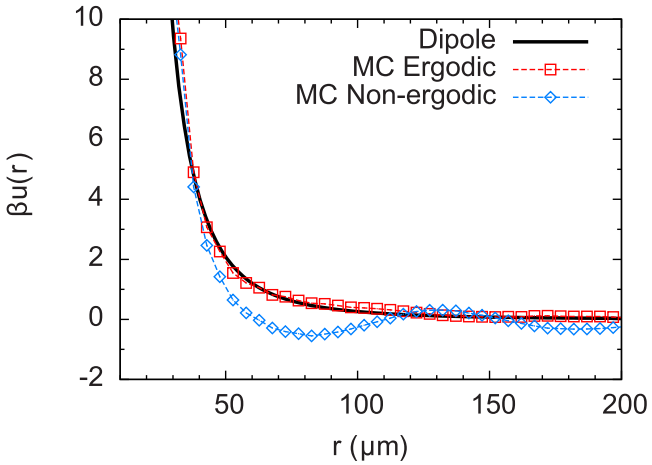

Figure 6. Effective interaction potentials obtained from an HDPC inversion of (*a*) ergodic (red points) and (*b*) non-ergodic (blue points) Monte-Carlo (MC) simulations of particles interacting through a dipolar potential $\beta U(r) = A/r^3$ with $A = 1.8 \times 10^5\ \mu\text{m}^3$ at a density of $\varphi = 1.05 \times 10^{-4}\ \mu\text{m}^{-2}$. The underlying dipole potential is plotted as a black curve for comparison.

4. Conclusions

Many physical mechanisms have been discussed and proposed in the literature to describe the interaction of charged particles confined to the two dimensional interface between a water solution and a low dielectric constant oil. These systems are both fundamentally interesting and relevant to applications. Without entering into the specific physics of these often complex models, we instead in this work focus on exploring experimentally whether a density-dependent interaction potential is required to explain the observed particle order beyond the dilute limit. This is a simpler and well defined question—and answering it would allow to discriminate between classes of models. We have described a number of subtle difficulties in answering even this simple question, and we have shown the usefulness of extracting pair potentials both from inversions and from the thermal fluctuation dynamics. Our conclusion is that the experimental data throughout the density regime is well described by the density independent, and simple, repulsive dipole form well known previously in dilute conditions.

Acknowledgments

We acknowledge useful discussions with D Vella, C P Royall, M Oettel, G G Fuller and J Vermant, and preliminary work by J Adams and H Chow. PC was funded by EU-ITN Comploids, AM by a Royal Society Newton International Fellowship.

Appendix A. Calculating the equilibrium MSD using harmonic lattice theory

In this appendix, we calculate the 1D equilibrium msd defined in equation (6) using Harmonic lattice theory [48]. To do this, we first calculate the 2D equilibrium msd defined by

$$\langle \Delta r^2 \rangle = \langle \Delta x^2 \rangle + \langle \Delta y^2 \rangle = \left\langle \left(\mathbf{r}_0 - \frac{1}{6} \sum_{l=1}^{6} \mathbf{r}_l \right)^2 \right\rangle \tag{A1}$$

where $\mathbf{r}_l$ is the 2D vector position of the l-th particle ($l = 0$ refers to the central colloidal particle, and $l = 1 \rightarrow 6$ refers to the particle's nearest neighbours) and $\langle \Delta x^2 \rangle$, $\langle \Delta y^2 \rangle$ are the 1D msd along the x and y Cartesian coordinate axes, respectively. Since the x and y directions are not defined with respect to specific crystal orientations in the experiments, we have $\langle \Delta x^2 \rangle = \langle \Delta y^2 \rangle$ so that the 1D msd can be readily calculated from the 2D msd using

$$\langle \Delta x^2 \rangle = \langle \Delta r^2 \rangle / 2. \tag{A2}$$

In order to calculate the 2D msd, it is convenient to decompose the vector positions of the colloidal particles into

$$\mathbf{r}_l = \mathbf{R}_l + \mathbf{u}\left(\mathbf{R}_l\right) \tag{A3}$$

where $\mathbf{R}_l = n_1 \mathbf{a}_1 + n_2 \mathbf{a}_2$ is the equilibrium vector position of the l-th particle (i.e. Bravais lattice site of the l-th particle) and $\mathbf{u}\left(\mathbf{R}_l\right)$ is the displacement vector of the l-th particle from its equilibrium position. Here $\mathbf{a}_1 = a(1, 0)$, $\mathbf{a}_2 = a\left(1/2, \sqrt{3}/2\right)$ are the basis vectors and a is the lattice constant of the hexagonal crystal. It is also useful to define the reciprocal lattice vectors $\mathbf{b}_1 = 2\pi\left(1, -1/\sqrt{3}\right)$, $\mathbf{b}_1 = 2\pi\left(0, 2/\sqrt{3}\right)$ which are defined such that $\mathbf{a}_i \cdot \mathbf{b}_j = 2\pi\delta_{ij}$ where δ_{ij} is the Kronecker delta. Inserting equation (A3) into equation (A1) and simplifying, the equilibrium 2D msd can be written in terms of the particle displacement vectors as

$$\langle \Delta r^2 \rangle = \frac{1}{36} \left\langle \left(\sum_{l=1}^{6} \mathbf{u}\left(\mathbf{R}_0\right) - \mathbf{u}\left(\mathbf{R}_l\right) \right)^2 \right\rangle. \tag{A4}$$

Next, we express the displacement vector as a Fourier series

$$u_j(\mathbf{R}) = \frac{1}{V} \sum_{\mathbf{q}} u_j(\mathbf{q}) \mathrm{e}^{\mathrm{i}\mathbf{q}\cdot\mathbf{R}} \tag{A5}$$

where $j = 1, 2$ refers to the x and y Cartesian components respectively of the displacement vector, V is the total area of the system, $u_j(\mathbf{q})$ is the Fourier transform of $u_j(\mathbf{R})$ and the sum runs over all allowed wavevectors $\mathbf{q} = \alpha\mathbf{b}_1 + \beta\mathbf{b}_2$. In the limit of infinite system size, all wavevectors within a reciprocal lattice unit cell are allowed, i.e. $0 \leqslant \alpha, \beta \leqslant 1$ [47]. Inserting equation (A5) into equation (A4) and setting $\mathbf{R}_0 = 0$ without loss of generality, we obtain

$$\langle \Delta r^2 \rangle = \frac{1}{36V^2} \sum_{j=1,2} \sum_{\mathbf{q},\mathbf{q}'} \langle u_j(\mathbf{q}) u_j(\mathbf{q}') \rangle \times \sum_{l,m} \left(1 - \mathrm{e}^{\mathrm{i}\mathbf{q}\cdot\mathbf{R}_l}\right)\left(1 - \mathrm{e}^{\mathrm{i}\mathbf{q}\cdot\mathbf{R}_m}\right). \tag{A6}$$

We next invoke the equipartition theorem for the different Fourier modes [49]

$$\frac{1}{V} \langle u_i(\mathbf{q}) u_j(\mathbf{q}') \rangle = k_\mathrm{B} T D_{ij}^{-1}(\mathbf{q}) \delta_{\mathbf{q},\mathbf{q}'} \tag{A7}$$

where $D_{ij}^{-1}(\mathbf{q})$ is the inverse of the Fourier space dynamical matrix $D_{ij}(\mathbf{q})$ which is given by [47]

$$D_{ij}(\mathbf{q}) = -\frac{2}{v_0} \sum_{\mathbf{R}} D_{ij}(\mathbf{R}) \sin^2\left(\frac{1}{2}\mathbf{q}\cdot\mathbf{R}\right) \tag{A8}$$

and $D_{ij}(\mathbf{R})$ is the real space dynamical matrix which is given by

$$D_{ij}(\mathbf{r}) = -\frac{\partial^2 U(\mathbf{r})}{\partial r_i \partial r_j}. \tag{A9}$$

In equation (A8), the sum runs over Bravais lattice sites $\mathbf{R} = n_1\mathbf{a}_1 + n_2\mathbf{a}_2$, i.e. over integer values of n_1, n_2 such that $n_1, n_2 \leqslant n_\mathrm{max}$, where n_max is the effective cut-off radius for the sum. Because $D_{ij}(\mathbf{r})$ decays rapidly with $\mathbf{r}$, a relatively small value of $n_\mathrm{max} = 5$ is sufficient to ensure good convergence. Also $v_0 = \sqrt{3}a^2/2$ is the area of the unit cell and it appears in equation (A8) because we are performing Fourier transforms of a function of a discrete variable, i.e. $D_{ij}(\mathbf{R})$ [49]. Inserting equation (A7) into equation (A6) and simplifying, we find

$$\langle \Delta r^2 \rangle = \frac{k_\mathrm{B} T}{V} \sum_{\mathbf{q}} \left[D_{xx}^{-1}(\mathbf{q}) + D_{yy}^{-1}(\mathbf{q}) \right] f(\alpha, \beta) \tag{A10}$$

where

$$f(\alpha, \beta) = \frac{1}{36} \sum_{l} \sum_{m} \left(1 - \mathrm{e}^{\mathrm{i}\mathbf{q}\cdot\mathbf{R}_l}\right)\left(1 - \mathrm{e}^{-\mathrm{i}\mathbf{q}\cdot\mathbf{R}_m}\right) = \frac{1}{9}\left(\cos 2\pi\alpha + \cos 2\pi\beta + \cos 2\pi(\alpha - \beta) - 3\right)^2. \tag{A11}$$

Finally, in the limit of infinite system size, we can replace the sum over $\mathbf{q}$ in equation (A10) by an integral over wavevectors $\mathbf{q}$ which lie within a unit cell of the reciprocal lattice [49]. Substituting equation (A10) into equation (A2) we obtain

$$\langle \Delta x^2 \rangle = \frac{k_\mathrm{B} T}{2} \int\int \frac{\mathrm{d}^2 q}{(2\pi)^2} \left[D_{xx}^{-1}(\mathbf{q}) + D_{yy}^{-1}(\mathbf{q}) \right] f(\alpha, \beta) = \frac{k_\mathrm{B} T}{v_0} \int_0^1 \int_0^1 \mathrm{d}\alpha \mathrm{d}\beta \left[D_{xx}^{-1}(\alpha, \beta) + D_{yy}^{-1}(\alpha, \beta) \right] f(\alpha, \beta). \tag{A12}$$

Inserting an interaction potential $U(\mathbf{r})$ into equations (A8), (A9) and (A12) allows us to calculate the equilibrium 1D msd as a function of density or lattice spacing a.

For dipole potentials given by equation (2) (or more generally power law potentials with an arbitrary exponent), it is possible to explicitly factor out the dependence of the equilibrium msd on the dipole strength A and lattice constant a (or equivalently density φ) by writing the real space dynamical matrix as

$$D_{ij}(\mathbf{r}) = \frac{Ak_{\mathrm{B}}T}{a^5}\tilde{D}_{ij}(\mathbf{r}/a) \tag{A13}$$

where $\tilde{D}_{ij}(\mathbf{r}/a)$ is the dimensionless real space dynamical matric that is independent of A and a. Substituting equation (A13) into equations (A8) and (A12), we find

$$\langle \Delta x^2 \rangle = \left\{ \frac{1}{2v_0} \int_0^1 \int_0^1 \mathrm{d}\alpha \mathrm{d}\beta \left[\tilde{D}_{xx}^{-1}(\alpha, \beta) + \tilde{D}_{yy}^{-1}(\alpha, \beta) \right] \times f(\alpha, \beta) \right\} \frac{a^5}{A} \tag{A14}$$

where $\tilde{D}_{ij}(\alpha, \beta)$ is the Fourier transform of the dimensionless real space dynamical matrix (obtained by replacing $D_{ij}(\mathbf{R})$ with $\tilde{D}_{ij}(\mathbf{R})$ in equation (A8)). The term inside the curly brackets is independent of A and a and can be explicitly evaluated, yielding equation (8).

Appendix B. Escape times of colloids in a colloidal monolayer

In this appendix, we estimate the escape time of a colloid from the cage formed by its nearest neighbours as a function of the monolayer density. To simplify our calculation, we assume that the colloidal monolayer is in a hexagonal crystal state and and that the interaction between colloids has the dipolar form given by equation (2), with $A = 1.8 \times 10^5\, \mu\mathrm{m}^3$. The escape time of a colloid from the cage formed by its six nearest neighbours can be estimated from

$$\tau_{\mathrm{escape}} = \tau_0 \mathrm{e}^{\beta \Delta U} \tag{B1}$$

where $\tau_0 = a^2/(4D_0)$ is the escape time for a free particle and ΔU is the energy barrier for the particle to escape from the cage. We can explicitly factor out the density dependence of the energy barrier by writing

$$\beta \Delta U = \frac{A}{a^3} \tilde{\Delta U} \tag{B2}$$

where $\tilde{\Delta U}$ is a dimensionless energy barrier that is independent of monolayer density.

We have estimated $\tilde{\Delta U}$ in two different ways. Firstly, by only accounting for the interaction of the colloid with its 6 nearest neighbours and assuming they are fixed in space, we estimated $\tilde{\Delta U}$ by calculating the energy barrier for the lowest energy 'pass' in the energy landscape. Secondly, we estimated $\tilde{\Delta U}$ from the simulation results of Aveyard *et al* [50] which takes into account a more realistic transitional state for the escaping colloid (see figure 8 of that paper). Interestingly, both approaches yield $\tilde{\Delta U} \approx 10$. Using $\tilde{\Delta U} \approx 10$ and $D_0 = 0.28\, \mu\mathrm{m}^2\, \mathrm{s}^{-1}$, the colloid escape time for different monolayer densities are given in table 2.

Table 2. Colloid escape times for colloidal monolayers of different densities.

$\varphi/\mu\mathrm{m}^{-2}$	$a/\mu\mathrm{m}$	$\tau_{\mathrm{escape}}/\mathrm{s}$
2.3×10^{-4}	71.6	6.1×10^{5}
7.3×10^{-4}	39.7	4.6×10^{15}
1.05×10^{-3}	33.0	4.5×10^{24}
1.8×10^{-3}	25.3	7.3×10^{50}
2.2×10^{-3}	15.5	7.8×10^{69}

From table 2, it is clear that the absolute numbers for the escape time are unrealistically large, suggesting that the value for $\tilde{\Delta U}$ that we have estimated from colloids in the crystal phase is unrealistic for colloids in the fluid phase. Notwithstanding this deficiency, the most interesting feature about the results in table 1 is the fact that there is a very strong dependence of τ_{escape} on density which is due to the strong density dependence in the exponent of equation (B1). We believe that this feature of the calculation is realistic and supports our claim that colloidal monolayers rapidly become non-ergodic as we increase density. We note in particular the huge increase in τ_{escape} going from $\varphi = 2.25 \times 10^{-4}\, \mu\mathrm{m}^{-2}$ to $\varphi = 7.33 \times 10^{-4}\, \mu\mathrm{m}^{-2}$, the latter being the density where we start to see a minima appearing in the inverted pair potential.

References

[1] Pieranski P 1980 *Phys. Rev. Lett.* **45** 569
[2] Aveyard R, Binks B P and Clint J H 2003 *Adv. Colloid Interface Sci.* **100** 503
[3] Vignati E, Piazza R and Lockhart T P 2003 *Langmuir* **19** 6650
[4] Melle S, Lask M and Fuller G G 2005 *Langmuir* **21** 2158
[5] Hunter R J 1986 *Foundations of Colloid Science* vol 1 (New York: Oxford University Press)
[6] Aveyard R *et al* 2002 *Phys. Rev. Lett.* **88** 246102
[7] Masschaele K, Park B, Furst E, Fransaer J and Vermant J 2010 *Phys. Rev. Lett.* **105** 048303
[8] Park B, Vermant J and Furst E 2010 *Soft Matter* **6** 5327
[9] Stillinger F H 1961 *J. Chem. Phys.* **35** 1584
[10] Hurd A 1985 *J. Phys. A: Math. Gen.* **18** L1055
[11] Oettel M and Dietrich S 2008 *Langmuir* **24** 1425
[12] Aveyard R, Clint J H, Ness D and Paunov V N 2000 *Langmuir* **16** 1969
[13] Nikolaides M G, Bausch A R, Hsu M F, Dinsmore A D, Brenner M P, Gay C and Weitz D A 2002 *Nature* **420** 299
[14] Chen W, Tan S S, Zhou Y, Ng T K, Ford W and Tong P 2009 *Phys. Rev.* E **79** 041403
[15] Oettel M, Domínguez A and Dietrich S 2005 *Phys. Rev.* E **71** 051401
[16] Park B J and Furst E 2011 *Soft Matter* **7** 7676
[17] Chen W, Tan S, Ng T, Ford W T and Tong P 2005 *Phys. Rev. Lett.* **95** 218301
[18] Domínguez A, Frydel D and Oettel M 2008 *Phys. Rev.* E **77** 020401
[19] Loudet J C, Alsayed A M, Zhang J and Yodh A G 2005 *Phys. Rev. Lett.* **94** 018301
[20] Cavallaro M Jr, Botto L, Lewandowski E P, Wang M and Stebe K J 2011 *Proc. Natl Acad. Sci. USA* **108** 20923
[21] Yao L, Botto L, Cavallaro M Jr, Bleier B J, Garbin V and Stebe K J 2013 *Soft Matter* **9** 779
[22] Aveyard R, Clint J H, Nees D and Quirke N 2000 *Langmuir* **16** 8820

[23] Stancik E J, Widenbrant M J O, Laschitsch A T, Vermant J and Fuller G G 2002 *Langmuir* **18** 4372
[24] Cicuta P, Stancik E J and Fuller G G 2003 *Phys. Rev. Lett.* **90** 236101
[25] Reynaert S, Moldenaers P and Vermant J 2006 *Langmuir* **22** 4936
[26] Maestro A, Bonales L, Ritacco H, Rubio R and Ortega F 2010 *Phys. Chem. Chem. Phys.* **12** 14115
[27] Maestro A, Guzman E, Ortega F and Rubio R 2014 *Curr. Opin. Colloid Interface Sci.* **19** 355–67
[28] Loudet J C, Yodh A G and Pouligny B 2006 *Phys. Rev. Lett.* **97** 018304
[29] Paunov V N 2003 *Langmuir* **19** 7970
[30] Isa L, Lucas F, Wepf R and Reimhult E 2011 *Nat. Commun.* **2** 1
[31] Leoni M, Kotar J, Bassetti B, Cicuta P and Cosentino Lagomarsino M 2009 *Soft Matter* **5** 472
[32] Cicuta P and Donald A M 2007 *Soft Matter* **3** 1449–55
[33] Likos C 2001 *Phys. Rep.* **348** 267
[34] Bolhuis P G, Louis A A and Hansen J P 2001 *Phys. Rev.* E **64** 021801
[35] Brunner M, Bechinger C, Strepp W, Lobaskin V and von Gruenberg H H 2002 *Europhys. Lett.* **58** 926
[36] Law A D and Buzza D M A 2009 *J. Chem. Phys.* **131** 094704
[37] Law A D and Buzza D M A 2010 *Langmuir* **26** 7107
[38] Frenkel D, Vos R J, de Kruif C G and Vrij A 1986 *J. Chem. Phys.* **84** 4625
[39] Rajagopalan R and Srinivasa Rao K 1997 *Phys. Rev.* E **55** 4423
[40] Quesada-Pérez M, Moncho-Jordá A, Martnez-López F and Hidalgo-Álvarez R 2001 *J. Chem. Phys.* **115** 10897
[41] Pusey P N 1991 *Liquids, Freezing and the Glass Transition* ed J P Hansen *et al* (Amsterdam: North-Holland)
[42] Mermin N D 1968 *Phys. Rev.* **176** 250
[43] Bedanov V M, Gadiyak G V and Lozovik Y E 1985 *Phys. Lett.* A **109** 289
[44] Zheng X H and Earnshaw J C 1998 *Europhys. Lett.* **41** 635
[45] Cui B, Lin B and Rice S A 2001 *J. Chem. Phys.* **114** 9142
[46] Chen K, Still T, Aptowicz K B, Schoenholz S, Schindler M, Maggs A C, Liu A J and Yodh A G 2013 *Phys. Rev.* E **88** 022315
[47] Ashcroft N W and Mermin N D 1976 *Solid State Physics* (Belmont, CA: Brooks/Cole)
[48] Keim P, Maret G, Herz U and von Grünberg H H 2004 *Phys. Rev. Lett.* **92** 215504
[49] Chaikin P M and Lubensky T C 2000 *Principles of Condensed Matter Physics* (Cambridge: Cambridge University Press)
[50] Aveyard R *et al* 2002 *Langmuir* **18** 9587